Journal of Power Sources 242 (2013) 208–215

Contents lists available at SciVerse ScienceDirect

Journal of Power Sources

journal homepage: www.elsevier.com/locate/jpowsour

Copper phthalocyanine functionalization of graphene nanosheets as support for platinum nanoparticles and their enhanced performance toward methanol oxidation

Jing-Ping Zhong [a], You-Jun Fan [a,*], Hui Wang [a], Rui-Xiang Wang [a], Li-Li Fan [a], Xing-Can Shen [a], Zu-Jin Shi [b]

[a] Key Laboratory for the Chemistry and Molecular Engineering of Medicinal Resources (Ministry of Education of China), College of Chemistry and Chemical Engineering, Guangxi Normal University, Guilin 541004, China
[b] Beijing National Laboratory for Molecular Sciences, College of Chemistry and Molecular Engineering, Peking University, Beijing 100871, China

HIGHLIGHTS

- A new Pt nanoparticles electrocatalyst using copper phthalocyanine (TSCuPc) functionalized graphene as support is reported.
- Pt nanoparticles with high electrochemical active surface area are uniformly deposited on the functionalized graphene surface.
- The Pt/TSCuPc–graphene catalyst exhibits much higher electrocatalytic activity and stability for methanol oxidation.

ARTICLE INFO

Article history:
Received 22 January 2013
Received in revised form
8 May 2013
Accepted 20 May 2013
Available online 28 May 2013

Keywords:
Direct methanol fuel cells
Graphene
Functionalization
Platinum
Anode catalyst

ABSTRACT

We herein report a facile and effective ultrasonication method to non-covalently functionalize graphene with copper phthalocyanine-3,4′,4″,4‴-tetrasulfonic acid tetrasodium salt (TSCuPc) as a promising catalyst support for Pt nanoparticles. With the assistance of TSCuPc, Pt nanoparticles are homogeneously deposited on the surface of graphene, and their dispersivity and electrochemical active surface area (ECSA) are obviously enhanced. Studies of cyclic voltammetry and chronoamperometry demonstrate that the as-prepared Pt/TSCuPc–graphene catalyst exhibits much higher electrocatalytic activity and stability than the Pt/graphene and commercial Pt/C catalysts for methanol oxidation. It is concluded that the strategy of TSCuPc-functionalized graphene with Pt catalysts will be potential in design and synthesis of the highly efficient electrocatalysts for DMFCs applications.

1. Introduction

Direct methanol fuel cells (DMFCs) have received much attention because of its advantages of low operating temperature, easy transportation and storage of fuel, high energy conversion efficiency and low pollution emission [1–4]. Nevertheless, the commercialization of DMFCs still faces serious problems such as poor kinetics of methanol oxidation, methanol crossover through the membrane and CO poisoning of the catalysts [5,6]. One of the keys to overcoming these barriers is to develop the anodic electrocatalysts with high performance. At present, the most commonly used electrocatalysts in DMFCs are Pt-based nanoparticles supported on carbon black (e.g., Vulcan XC72) [7,8]. In spite of their high surface area and good electrochemical performance, low Pt utilization and significantly high cost of the catalysts remain unresolved. In recent years, extensive efforts have been devoted to finding various new carbon supports such as carbon nanotubes [9,10], carbon nanofibers [11], ordered mesoporous carbon [6,12], carbon nanospheres [13] and graphene [14–20] to obtain the high dispersion and electrochemical active surface area (ECSA) of Pt nanoparticles. It is worth noting that, among those carbon materials, graphene with an atom-thick two-dimensional plane structure has attracted particular attention due to its theoretically large surface area, excellent electrical conductivity, good chemical, thermal, optical and electrochemical stabilities and low cost [21]. For instance, Dong et al. loaded Pt and PtRu nanoparticles

* Corresponding author. Tel.: +86 773 5846279; fax: +86 773 2120958.
E-mail address: youjunfan@mailbox.gxnu.edu.cn (Y.-J. Fan).

0378-7753/$ – see front matter © 2013 Elsevier B.V. All rights reserved.
http://dx.doi.org/10.1016/j.jpowsour.2013.05.085

on graphene sheets, which exhibited enhanced efficiency for both methanol and ethanol oxidation compared to the catalysts supported on Vulcan XC-72R carbon black [15]. Xin et al. prepared Pt/graphene catalyst with higher electrocatalytic activity and stability for methanol oxidation by the $NaBH_4$ reduction route [17]. More recently, Yu et al. fabricated a novel CeO_2/rGO/Pt sandwich nanostructure through a facile hydrothermal approach, the electrochemical tests indicated that this structure exhibited higher methanol oxidation activity and stability than the Pt/rGO, CeO_2/Pt and Pt/C catalysts [20]. Unfortunately, pristine graphene is insoluble in organic solvents and susceptible to aggregation in aqueous solutions, which greatly hinders its practical applications in the preparation of graphene-based catalysts [21,22]. Therefore, it is necessary to further functionalize graphene sheets in order to improve their surface properties and dispersions in solvents.

The functionalization of graphene can be performed by covalent or non-covalent methods [23–26]. Covalent functionalization is commonly carried out by reacting acid-treated graphene containing hydroxyl (–OH) and carboxyl (–COOH) groups with functional molecules, which will have a significant effect on the electronic properties of graphene. Non-covalent functionalization is preferable for catalyst support applications, since it enables attachment of molecules through supermolecular interactions such as π–π stacking, electrostatic interaction and hydrogen bonding, and thus preserves the intrinsic electronic and structural properties of graphene. Metal phthalocyanines (MPcs), the two-dimensional 18 π-electron aromatic macrocycles with a metal atom located at the central cavity, are of great interest due to their excellent electronic properties and potential applications in some fields such as electrical devices, solar cells and biosensors [27–30]. Very recently, several research groups have explored MPcs functionalized graphene composites for the achievement of dispersed graphene and the cathode electrode materials of fuel cells [30–34]. Mensing et al. reported the electrochemical production of a stable aqueous dispersion of graphene–copper phthalocyanine hybrid material [32]. Zhang et al. prepared iron tetrasulfophthalocyanine functionalized graphene composites with enhanced activity for the oxygen reduction reaction (ORR) in a dual-chamber microbial fuel cell [33]. Zhang et al. also reported the synthesis of iron phthalocyanine and nitrogen-doped graphene composite, which exhibited superior ORR catalytic activity and excellent tolerance to methanol crossover [34]. However, to the best of our knowledge, MPcs functionalized graphene composites used as the anodic catalyst support of fuel cells have not yet been reported.

Herein, for the first time, we report a facile and effective ultrasonication approach to non-covalently functionalize graphene with copper phthalocyanine-3,4′,4″,4‴-tetrasulfonic acid tetrasodium salt (TSCuPc) as a promising catalyst support for Pt nanoparticles. The prepared nanocomposites were characterized by UV–vis absorption spectroscopy, Raman spectroscopy, X-ray diffraction (XRD), thermogravimetric analysis (TGA), transmission electron microscopy (TEM) and energy dispersive X-ray (EDX) spectroscopy. The electrocatalytic activity and durability of the Pt/TSCuPc–graphene catalyst were evaluated by cyclic voltammetry (CV) and chronoamperometry methods. Results demonstrate that the Pt/TSCuPc–graphene exhibits much higher electrocatalytic activity and stability than the Pt/graphene and commercial Pt/C catalysts for methanol oxidation. The present work provides a promising strategy to design and fabricate the highly efficient graphene-based electrocatalysts for DMFCs applications.

2. Experimental

2.1. Materials

Graphene sheets (99.95%) used there was prepared by direct current arc-discharge method as reported in our previous work [35]. 5 wt% Nafion solution and copper (II) phthalocyanine-3,4′,4″,4‴-tetrasulfonic acid tetrasodium salt (TSCuPc) were purchased from Sigma–Aldrich. Hydrogen hexachloroplatinate (IV) hexahydrate ($H_2PtCl_6 \cdot 6H_2O$), methanol and sulfuric acid were obtained from Sinopharm Chemical Reagent Co. Ltd (Shanghai, China), and commercial Pt/C catalyst (20% Pt loading) was supplied from Alfa Aesar. All the chemicals are of analytical grade and used as received without further purification. All aqueous solutions were prepared using triple-distilled water.

2.2. Preparation of Pt/TSCuPc–graphene catalyst

Scheme 1 briefly illustrates the preparation process of Pt/TSCuPc–graphene catalyst. 10 mg graphene and 25 mg TSCuPc were dispersed in 8 mL triple-distilled water by ultrasonic treatment for 6 h, and then the as-obtained suspension was allowed to stand overnight. Subsequently, 665 μL H_2PtCl_6 solution (19 mM) was added into the suspension in 30 min with ultrasonication, and the pH value of system was adjusted to 10.5 by NaOH solution. An excess quantity of $NaBH_4$ solution (10 mg mL^{-1}) was then slowly added dropwise into the above solution under ultrasonication. After reaction for 6 h under ultrasonication, the resulting black solid product were collected by centrifugation, washed repeatedly with triple-distilled water and absolute ethanol several times to remove the ions possibly remaining in the final product, and then dried in vacuum at 40 °C for 24 h. For comparison, Pt nanoparticles supported on graphene (Pt/graphene) was prepared with the similar procedure as described above.

2.3. Physical characterization

2.3.1. UV–vis absorption spectroscopy, Raman spectroscopy and thermogravimetric analysis (TGA)

UV–vis absorption spectra were recorded by a UV–vis spectrophotometer (Varian-Cary 100, USA). The samples were dissolved in triple-distilled water prior to the UV–vis spectroscopy measurements. Raman spectra were obtained by a confocal microscopic Raman spectrometer (Renishaw-InVia, UK), using an argon ion laser with a wavelength of 514.5 nm. Thermogravimetric analysis

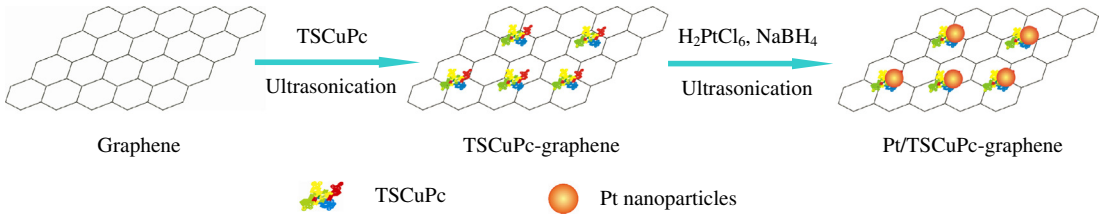

Scheme 1. Schematic illustration of the preparation process of Pt/TSCuPc–graphene catalyst.

(TGA) was performed on a simultaneous thermogravimetric analyzer (Labsysevo TG-DSC/DTA, France). The samples were heated under a nitrogen atmosphere from room temperature to 1000 °C at a rate of 10 °C min^{-1}.

2.3.2. X-ray diffraction (XRD)

X-ray diffraction (XRD) was carried out on an X-ray diffractometer (Rigaku D/MAX 2500 v/pc, Japan) with a Cu Kα radiation source (λ = 1.5406 Å) generated at 40 kV and 100 mA. The XRD patterns were obtained at a scanning rate of 5° min^{-1} for 2θ values between 10° and 90°.

2.3.3. Transmission electron microscopy (TEM)

The size and morphology of the prepared catalysts were analyzed by high-resolution transmission electron microscope (HRTEM, JEOL JEM-2100) with an accelerating voltage of 200 kV. TEM specimens were prepared by ultrasonically dispersing the catalyst powder in ethanol. A drop of the suspension was deposited on a Cu grid coated with carbon film and allowed to dry before being inserted into the microscope. The size distribution of catalysts was evaluated statistically by measuring the diameter of 200 Pt nanoparticles in the magnified TEM images. Energy dispersive X-ray (EDX) spectroscopy characterization was carried out on the same apparatus (JEOL JEM-2100).

2.3.4. Composition analysis of catalysts

To measure and compare the activity based on the Pt mass, an inductively coupled plasma-optical emission spectrophotometer (ICP-OES, Thermo Electron IRIS Intrepid II XSP, USA) was employed for composition measurements. The plasma conditions for Pt analysis were as follows: RF power: 1150 W, Nebulizer pressure: 28.0 psi, Auxiliary gas (Ar) flow rate: 1.0 L min^{-1}. The samples were first dissolved with aqua regia, and then the mixtures were filtered in order to remove the undissolved graphene material. In this study, the Pt contents of as-prepared Pt/TSCuPc–graphene and Pt/graphene catalysts were determined to be 11.9% and 15%, respectively.

2.4. Electrochemical measurements

The electrochemical measurements were conducted at room temperature around 25 °C using a standard three-electrode cell connected to a CHI 660D electrochemical workstation. The counter electrode was a piece of Pt foil (1 cm^2) and a saturated calomel electrode (0.259 V relative to reversible hydrogen electrode, RHE) was used as reference electrode. All potentials in the electrochemical tests are quoted versus the RHE scale. The working electrode is prepared as follows: the glass carbon (GC, Φ = 5 mm) electrode, polished with 5.0 μm, 1.0 μm, 0.3 μm Al_2O_3 slurry and washed ultrasonically in water and ethanol for 5 min, respectively, was used as substrate for the catalysts. Then 1.5 mg of the as-prepared catalyst was dispersed ultrasonically in 400 μL Nafion solution (0.5 wt%), and 10 μL of the mixture was pipetted and air-dried on the pretreated GC electrode at room temperature.

The ECSA of Pt nanoparticles was calculated from the hydrogen adsorption/desorption curve, which was recorded in 0.5 M H_2SO_4 solution at a scan rate of 50 mV s^{-1}. The electrocatalytic performance of catalysts toward methanol oxidation was studied in 0.5 M CH_3OH + 0.5 M H_2SO_4 solution. CO stripping voltammograms were obtained by oxidizing preadsorbed CO in 0.5 M H_2SO_4 solution at a scan rate of 50 mV s^{-1}. CO was bubbled into 0.5 M H_2SO_4 for 10 min to allow saturated adsorption of CO onto the catalyst while maintaining the potential scan between 0.059 and 0.259 V, and then the dissolved CO in the electrolyte was removed by purging with nitrogen for 20 min. The current density in the electrochemical test was expressed by the normalized current per milligram of Pt loading. Before each electrochemical experiment, the electrolytic solution was purged with nitrogen for 15 min, and a flux of nitrogen was kept over the solution during measurements to prevent the interference of atmospheric oxygen.

3. Results and discussion

To confirm TSCuPc immobilization on the surface of graphene, the prepared nanocomposites were characterized in an aqueous solution by UV–vis absorption spectroscopy and the results were shown in Fig. 1A. It can be seen that TSCuPc exhibits strong absorbance (curve a) in the region 550–700 nm when compared to graphene without the characteristic spectrum (curve b), corresponding to a HOMO–LUMO transition (Q-band) [28,32,36]. The Q-band in the dilute aqueous solution is split in two, with contributions from both aggregate absorption (~631 nm) and monomer absorption (~667 nm). On the other hand, the addition of graphene to TSCuPc significantly results in decreases in the intensity for the two peaks of Q-band, accompanied by a red-shift of 2 and 8 nm, respectively (curve c). These results suggest the π–π interaction between graphene and TSCuPc in the TSCuPc–graphene [32]. The decrease in the peak intensities should be due to a small amount of TSCuPc molecules attached to graphene and a decrease in the density of trapped electrons in TSCuPc [28,37]. Interestingly, after the deposition of Pt nanoparticles on the TSCuPc–graphene surface (curve d), two peaks of the composite are blue-shifted to some extent with respect to those of the TSCuPc–graphene, which

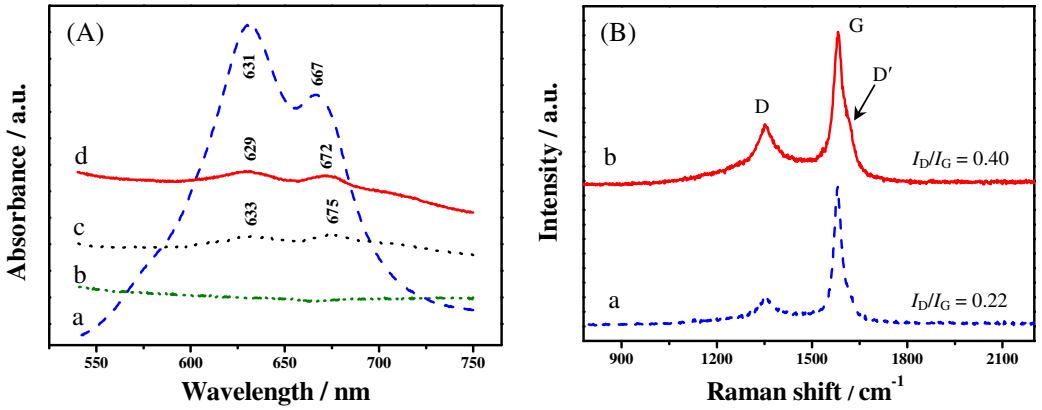

Fig. 1. (A) UV–vis absorption spectra of TSCuPc (a), graphene (b), TSCuPc–graphene (c) and Pt/TSCuPc–graphene (d) in aqueous solution. (B) Raman spectra of graphene (a) and TSCuPc–graphene (b).

might be attributed to the interaction between the Pt nanoparticles and TSCuPc–graphene support.

The surface-functionalization of graphene was also characterized by Raman spectroscopy. Fig. 1B displays the Raman spectra of graphene and TSCuPc–graphene. We can see that, both samples show two bands near 1353 and 1580 cm^{-1}, corresponding to the D and G bands, respectively [38,39]. The D band is assigned to the A_{1g} breathing mode of a disordered graphite structure, whereas the G band indicates the presence of E_{2g} structure mode of crystalline graphite. The D′ band, which is a shoulder of the G band at about 1616 cm^{-1}, corresponds to second-order Raman scattering from the variation of the D band [40]. The ratio of the intensities of the two bands (I_D/I_G) can be used to indicate the level of functionalization in a carbon material [41]. The I_D/I_G ratios for the pristine graphene and TSCuPc–graphene are 0.22 and 0.40, respectively. The higher I_D/I_G ratio and enhanced D′ band of the TSCuPc–graphene should be associated with a decrease in the average size of the sp^2 domains in the composite, which is caused by the non-covalent attachment of TSCuPc to the graphene surface [39].

In order to evaluate the thermal stability of TSCuPc, graphene and TSCuPc–graphene composite, TGA was performed under a nitrogen atmosphere. As can be seen from Fig. 2A, the TGA curve of TSCuPc shows two major weight loss steps from room temperature to 230 °C and from 440 to 530 °C (curve a), which might be due to the desorption of adsorbed water and the thermal decomposition of TSCuPc, respectively [42–44]. Furthermore, the TGA curve of pristine graphene (curve b) shows an obvious weight loss of around 37.3% at 900 °C, which excludes initial weight losses resulting from adsorbates [45]. As for the TSCuPc–graphene composite (curve c), it exhibits a weight loss at 440–600 °C, which might be attributed to the decomposition of TSCuPc on the graphene surfaces [44]. It is noted that the composite only shows a weight loss of 6.2% at 900 °C, suggesting that the amount of TSCuPc attached to the graphene sheets is small and as-prepared TSCuPc–graphene composite has good thermal stability.

Fig. 2B shows the XRD patterns of Pt/TSCuPc–graphene and Pt/graphene nanocomposites. The (002) peak located at the 2θ value of around 25.9° in both catalysts evidently originates from the layered structure of graphene support [46,47]. The five other diffraction peaks at 39.7°, 46.2°, 67.5°, 81.4° and 86.1° can be ascribed to the diffractions of Pt(111), Pt(200), Pt(220), Pt(311) and Pt(222) planes, respectively, which represent the characteristics of face-centered cubic (fcc) structure of platinum [7,19,48]. The average crystallite sizes of Pt nanoparticles were estimated by the Scherrer's equation based on the peak assigned to the (220) plane [19]. The (220) plane was chosen for the calculation since this peak does not overlap with other peaks and therefore allows accurate analyses. The crystallite sizes are determined to be 4.3 and 5.9 nm for Pt/TSCuPc–graphene and Pt/graphene, respectively.

The formation of the Pt/TSCuPc–graphene nanocomposite was further characterized by energy dispersive X-ray (EDX) spectroscopy, as shown in Fig. 3. The EDX spectrum shows the peaks corresponding to C, N, O, S, and Pt elements, confirming the deposition of Pt nanoparticles on the surface of TSCuPc functionalized graphene nanosheets.

The TEM image of Pt/TSCuPc–graphene catalyst is shown in Fig. 4A and the corresponding histogram of size distribution is shown in Fig. 4B. We can see that, most of the Pt nanoparticles were uniformly dispersed in the range of 3–7 nm on the TSCuPc–graphene support. The average particle size of Pt revealed by the size distribution histogram was approximately 4.6 nm, which was close to the XRD result. The TEM image of Pt/graphene catalyst is shown in Fig. 4C and the corresponding histogram of size distribution is shown in Fig. 4D. Most of the Pt nanoparticles were poorly dispersed on the graphene support with a broad size distribution. The average particle size of Pt revealed by the size distribution histogram was approximately 5.8 nm, which was also close to the XRD result. These results imply that the immobilization of TSCuPc on the graphene sheets produces the uniform distribution of surface functional groups, which are beneficial to the deposition of Pt nanoparticles.

The ECSA provides information regarding the number of available electrochemically active sites which is essential for understanding the utilization and electrocatalytic activity of Pt in the

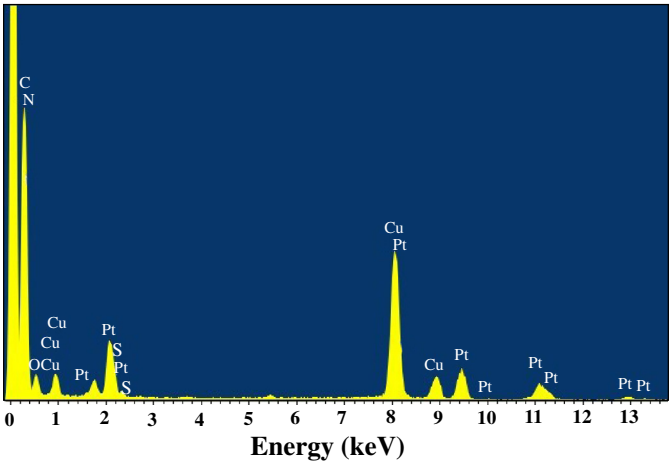

Fig. 3. EDX spectrum of the Pt/TSCuPc–graphene catalyst.

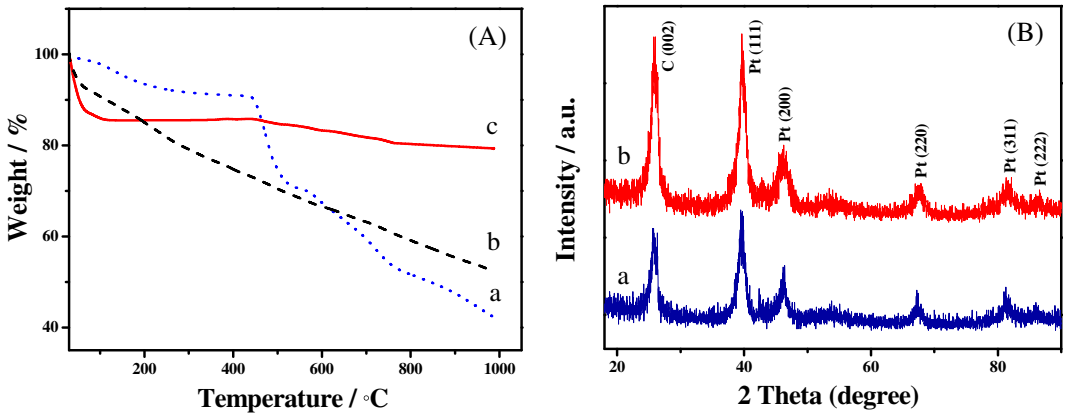

Fig. 2. (A) TGA curves of TSCuPc (a), graphene (b) and TSCuPc–graphene (c) under the protection of N_2. (B) XRD patterns of Pt/graphene (a) and Pt/TSCuPc–graphene (b) catalysts.

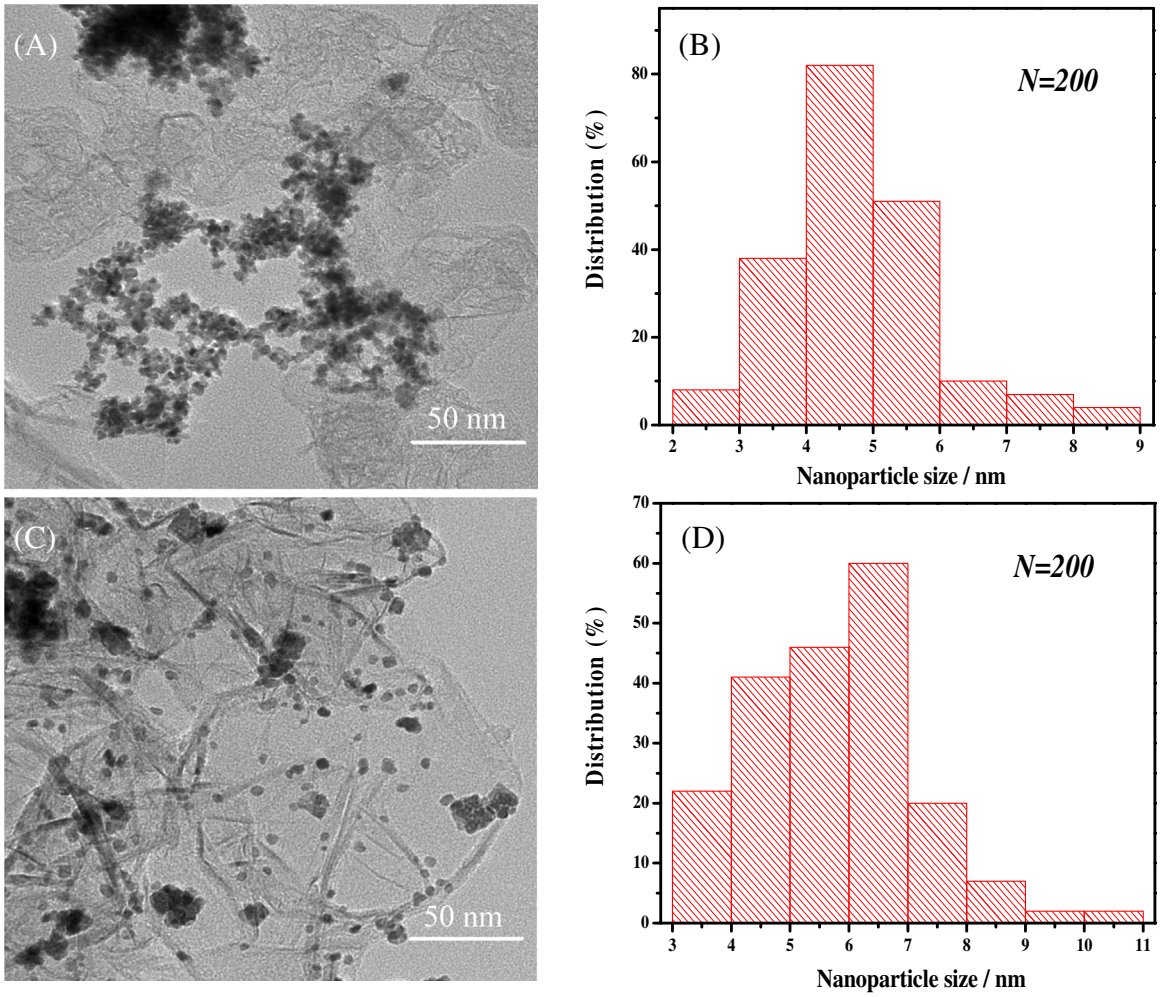

Fig. 4. TEM image (A) and the size distribution histogram (B) of Pt/TSCuPc–graphene catalyst. TEM image (C) and the size distribution histogram (D) of Pt/graphene catalyst.

resultant Pt/TSCuPc–graphene catalyst. Fig. 5 presents the cyclic voltammograms of Pt/TSCuPc–graphene, Pt/graphene and commercial Pt/C catalysts in nitrogen-saturated 0.5 M H_2SO_4 solution. Clearly, in addition to the current peaks for the formation and reduction of Pt oxide, the current peaks between 0.059 and 0.359 V

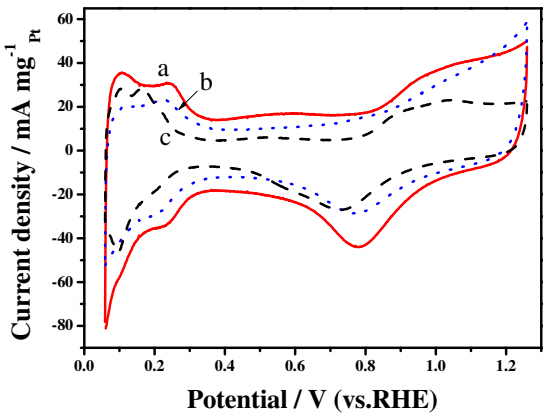

Fig. 5. Cyclic voltammograms of Pt/TSCuPc–graphene (a), Pt/graphene (b) and commercial Pt/C (c) catalysts in nitrogen-saturated 0.5 M H_2SO_4 solution at a scan rate of 50 mV s^{-1}.

are obviously observed, which are ascribed to the hydrogen adsorption/desorption behaviors at the electrodes. The ECSA is calculated from measuring the hydrogen adsorption/desorption charges after double-layer correction and assuming a value of 210 μC cm^{-2} for the adsorption of a hydrogen monolayer [13]. Therefore, the ECSA of Pt/TSCuPc–graphene catalyst can be calculated as 42.86 m^2 g^{-1}, higher than that of the Pt/graphene (31.46 m^2 g^{-1}) and Pt/C catalyst (39.72 m^2 g^{-1}), suggesting that the TSCuPc functionalization on graphene sheets causes a higher dispersion and utilization of Pt nanoparticles. It will be responsible for the superior electrocatalytic performance of Pt/TSCuPc–graphene catalyst discussed below.

Fig. 6A compares cyclic voltammograms of Pt/TSCuPc–graphene, Pt/graphene and commercial Pt/C catalysts in 0.5 M CH_3OH + 0.5 M H_2SO_4 solution. As can be seen, the voltammograms are similar to those reported in the literature [6,13,20], with two irreversible current peaks during the methanol oxidation, attributing to methanol oxidation (forward scan peak at around 0.879 V) and the oxidative removal of adsorbed intermediate species formed in the forward scan (backward scan peak at 0.659 V) [7,49]. The peak current densities of methanol oxidation on the Pt/TSCuPc–graphene catalyst (curve a) in the forward potential scan and in the backward potential scan are 730.3 and 571.5 mA mg^{-1}, respectively, much higher than those on the Pt/graphene (curve b, 212.6 and 200.7 mA mg^{-1}) and commercial Pt/C (curve c, 191.7 and

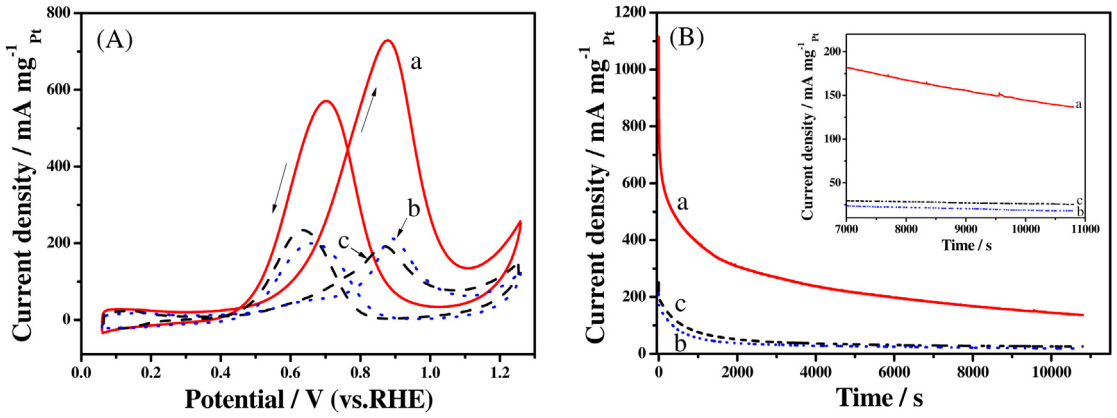

Fig. 6. (A) Cyclic voltammograms (50 mV s^{-1}) and (B) current–time curves, measured at 0.759 V, of methanol oxidation on Pt/TSCuPc–graphene (a), Pt/graphene (b) and commercial Pt/C (c) catalysts in 0.5 M CH_3OH + 0.5 M H_2SO_4 solution.

237.4 mA mg^{-1}) catalysts. Typically, the peak current density of Pt/TSCuPc–graphene in the forward scan is about 3.4 and 3.8 times that of the Pt/graphene and Pt/C catalysts, respectively. It should be noted that the mass activity of the Pt/TSCuPc–graphene is also higher than that of recent state-of-art Pt-based nanomaterials such as Pt/PAMAM/ACS composite [13], CeO_2/rGO/Pt sandwich nanostructure [20], PtRu–NP/CNT-PCA nanohybrid [50], Pt NPs@POM–GNS nanohybrid [51], and Pt NPs supported on surface-functionalized graphene [52], etc. Lu et al. reported the electrocatalytic properties of carbon supported cobalt phthalocyanine–platinum (CoPc-Pt/C) for methanol oxidation [53], but its mass activity is much lower than that of our Pt/TSCuPc–graphene catalyst. Additionally, it is interesting to observe that the onset potential of methanol oxidation on the Pt/TSCuPc–graphene (curve a) is 0.359 V which is lower than that on the Pt/graphene (curve b, 0.399 V) and Pt/C (curve c, 0.429 V) catalysts. These results strongly indicate that the electrocatalytic activity of the Pt/TSCuPc–graphene for methanol oxidation is much higher than that of the Pt/graphene and commercial Pt/C catalysts. It is well known that the ratio of the forward oxidation peak current (I_f) to the backward current peak (I_b), I_f/I_b, is generally used to describe the tolerance of catalysts to the accumulation of intermediate carbonaceous species during the methanol oxidation [7,19,54]. A higher ratio indicates an excellent oxidation of methanol in the forward scan and less accumulation of residues on the catalyst surface. Notably, the I_f/I_b ratio of Pt/TSCuPc–graphene catalyst (1.28) is higher than that of the Pt/graphene (1.06) and Pt/C (0.81) catalysts, showing better catalyst tolerance of the Pt/TSCuPc–graphene.

In order to compare the long-term electrochemical stability of Pt/TSCuPc–graphene, Pt/graphene and commercial Pt/C catalysts in methanol oxidation reactions, the chronoamperometric measurements were carried out in 0.5 M CH_3OH + 0.5 M H_2SO_4 solution at 0.759 V for 10,800 s. As shown in Fig. 6B, in all current–time curves, the initial current is dropped rapidly in the first 300 s, and then followed by a slower attenuation. The initial fast decay can be ascribed to the formation of intermediate species, such as CO_{ads}, CH_3OH_{ads} and CHO_{ads} during the methanol oxidation reaction [13,55]. The slow attenuation at longer times is due to the adsorption of sulfate anions on the surface of the catalysts [56,57]. After long-time operation, although the current gradually decays for all the catalysts, the Pt/TSCuPc–graphene maintains a much higher current (curve a), and the final current density is 137.6 mA mg^{-1}, which is almost 7.4 and 5.5 times that of the Pt/graphene (curve b, 18.5 mA mg^{-1}) and Pt/C (curve c, 25.2 mA mg^{-1}) catalysts, respectively, illustrating that the Pt/TSCuPc–graphene catalyst exhibits higher electrocatalytic activity and stability for methanol oxidation.

The CO-tolerance abilities of the catalysts were also evaluated by CO-stripping experiment. Fig. 7 shows the CO-stripping voltammograms for different catalysts. It can be seen that prior to the oxidation of adsorbed CO, the hydrogen adsorption/desorption is completely suppressed in all curves (the solid line), but the peaks associated with hydrogen adsorption/desorption appear after the removal of adsorbed CO (the dash line). The peak potential of CO oxidation on the Pt/TSCuPc–graphene catalyst (Fig. 7A) is negatively shifted to 0.779 V, while the potentials are 0.819 V and 0.859 V on the Pt/graphene (Fig. 7B) and Pt/C (Fig. 7C) catalysts, respectively. These results demonstrate that the introduction of TSCuPc in the Pt/TSCuPc–graphene effectively promotes the CO oxidation ability of the catalyst, which are in agreement with the above discussions.

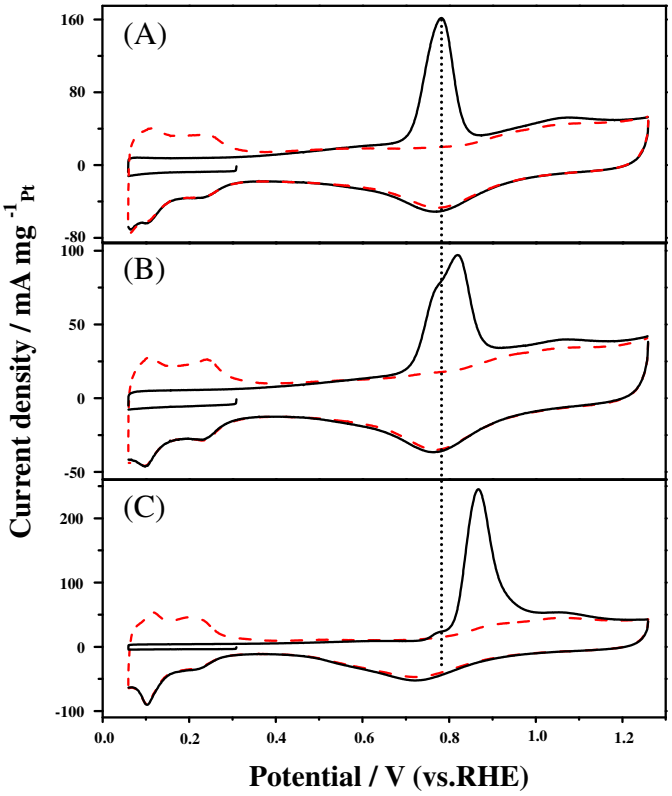

Fig. 7. CO stripping voltammograms of Pt/TSCuPc–graphene (A), Pt/graphene (B) and commercial Pt/C (C) catalysts in 0.5 M H_2SO_4 at a scan rate of 50 mV s^{-1}.

The significant enhancement in the electrocatalytic performances of Pt/TSCuPc–graphene catalyst for methanol oxidation maybe attributed to three major aspects: Firstly, the size and dispersion of Pt nanoparticles supported on the TSCuPc–graphene are obviously improved. The TSCuPc functionalization of graphene not only remarkably enhanced the solubility of graphene but also introduced homogeneous surface functional groups on the graphene surface. The increase in active triple-phase boundaries should be beneficial to the deposition of Pt nanoparticles with small size and high dispersion [58,59]. Secondly, the MPcs possess the unique molecular structure and outstanding physicochemical properties, such as exceptional thermal and chemical stability, and astounding electronic and photophysical features [32,60,61]. Zhou et al. revealed the promotion effect of steric hindrance and abundant electrons of iron tetrasulfophthalocyanine for formic acid oxidation [62]. It is reasonable to suggest that the synergistic effects between TSCuPc and Pt nanoparticles facilitate the methanol oxidation reaction, improving the electrochemical response of the composite catalyst. Finally, the sulfonic acid groups of TSCuPc can increase the hydrophilicity of the graphene by forming strong hydrogen bonds with water molecules, which promote their dissociation to produce $-OH_{ads}$ during the methanol oxidation reaction [50,63]. Consequently, the more $-OH_{ads}$ are created by the dissociative process, the more efficient the oxidation of intermediate species generated in methanol oxidation are.

4. Conclusions

In summary, a facile and effective ultrasonication approach to synthesize the Pt/TSCuPc–graphene catalyst by noncovalently functionalizing graphene with TSCuPc is reported here. In the presence of TSCuPc, Pt nanoparticles are uniformly deposited on the surface of graphene, and their dispersivity and ECSA value are obviously enhanced. The cyclic voltammetry and chronoamperometry tests demonstrate that the as-prepared Pt/TSCuPc–graphene catalyst exhibits much higher electrocatalytic activity and stability than the Pt/graphene and commercial Pt/C catalysts for methanol oxidation. This study provides a new synthesis strategy of Pt/graphene catalysts, which can be used to design and fabricate other graphene-based nanocomposites, thus allowing the development of the highly efficient electrocatalysts for DMFCs applications.

Acknowledgments

This work was supported by the National Natural Science Foundation of China (21263002, 21161003), Guangxi Natural Science Foundation of China (2013GXNSFAA019024, 2010GXNSFF013001) and the Foundation Project of Key Laboratory for the Chemistry and Molecular Engineering of Medicinal Resources (Guangxi Normal University), Ministry of Education of China (CMEMR2012-A3).

References

[1] Z.C. Tang, G.X. Lu, J. Power Sources 162 (2006) 1067–1072.
[2] D.R. Ou, T. Mori, H. Togasaki, M. Takahashi, F. Ye, J. Drennan, Langmuir 27 (2011) 3859–3866.
[3] X.S. An, Y.J. Fan, D.J. Chen, Q. Wang, Z.Y. Zhou, S.G. Sun, Electrochim. Acta 56 (2011) 8912–8918.
[4] Z.B. Wang, C.R. Zhao, P.F. Shi, Y.S. Yang, Z.B. Yu, W.K. Wang, G.P. Yin, J. Phys. Chem. C 114 (2010) 672–677.
[5] H.S. Liu, C.J. Song, L. Zhang, J.J. Zhang, H.J. Wang, D.P. Wilkinson, J. Power Sources 155 (2006) 95–110.
[6] J.R.C. Salgado, F. Alcaide, G. Álvarez, L. Calvillo, M.J. Lázaro, E. Pastor, J. Power Sources 195 (2010) 4022–4029.
[7] J.D. Qiu, G.C. Wang, R.P. Liang, X.H. Xia, H.W. Yu, J. Phys. Chem. C 115 (2011) 15639–15645.
[8] E. Antolini, Appl. Catal. B 88 (2009) 1–24.
[9] C. Paoletti, A. Cemmi, L. Giorgi, R. Giorgi, L. Pilloni, E. Serra, M. Pasquali, J. Power Sources 183 (2008) 84–91.
[10] C. Zhou, F. Peng, H. Wang, H. Yu, J. Yang, X. Fu, Fuel Cells 11 (2011) 301–308.
[11] Z. Lin, L.W. Ji, X.W. Zhang, Electrochim. Acta 54 (2009) 7042–7047.
[12] S.H. Joo, C. Pak, D.J. You, S.A. Lee, H.I. Lee, J.M. Kim, H. Chang, D. Seung, Electrochim. Acta 52 (2006) 1618–1626.
[13] Y.Q. Huang, H.L. Huang, Y.J. Liu, Y. Xie, Z.R. Liang, C.H. Liu, J. Power Sources 201 (2012) 81–87.
[14] Y.M. Li, L.H. Tang, J.H. Li, Electrochem. Commun. 11 (2009) 846–849.
[15] L.F. Dong, R.R.S. Gari, Z. Li, M.M. Craig, S.F. Hou, Carbon 48 (2010) 781–787.
[16] N.G. Shang, P. Papakonstantinou, P. Wang, S.R.P. Silva, J. Phys. Chem. C 114 (2010) 15837–15841.
[17] Y.C. Xin, J.G. Liu, Y. Zhou, W.M. Liu, J. Gao, Y. Xie, Y. Yin, Z.G. Zou, J. Power Sources 196 (2011) 1012–1018.
[18] Y.P. Xiao, S. Wan, X. Zhang, J.S. Hu, Z.D. Wei, L.J. Wan, Chem. Commun. 48 (2012) 10331–10333.
[19] Y.J. Li, W. Gao, L.J. Ci, C.M. Wang, P.M. Ajayan, Carbon 48 (2010) 1124–1130.
[20] X. Yu, L. Kuai, B.Y. Geng, Nanoscale 4 (2012) 5738–5743.
[21] C.C. Huang, C. Li, G.Q. Shi, Energy Environ. Sci. 5 (2012) 8848–8868.
[22] L. Yan, Y.B. Zheng, F. Zhao, S.J. Li, X.F. Gao, B.Q. Xu, P.S. Weiss, Y.L. Zhao, Chem. Soc. Rev. 41 (2012) 97–114.
[23] K.S. Subrahmanyam, A. Ghosh, A. Gomathi, A. Govindaraj, C.N.R. Rao, Nanosci. Nanotechnol. Lett. 1 (2009) 28–31.
[24] S. Niyogi, E. Bekyarova, M.E. Itkis, J.L. McWilliams, M.A. Hamon, R.C. Haddon, J. Am. Chem. Soc. 128 (2006) 7720–7721.
[25] X. Zhang, Y. Feng, S. Tang, W. Feng, Carbon 48 (2010) 211–216.
[26] W.W. Tu, J.P. Lei, S.Y. Zhang, H.X. Ju, Chem. Eur. J. 16 (2010) 10771–10777.
[27] S.S. Roy, D.J. Bindl, M.S. Arnold, J. Phys. Chem. Lett. 3 (2012) 873–878.
[28] R.A. Hatton, N.P. Blanchard, V. Stolojan, A.J. Miller, S.R.P. Silva, Langmuir 23 (2007) 6424–6430.
[29] I. Balan, I.G. David, V. David, A.I. Stoica, C. Mihailciuc, I. Stamatin, A.A. Ciucu, J. Electroanal. Chem. 654 (2011) 8–12.
[30] H.S. Yin, Y.L. Zhou, J. Xu, S.Y. Ai, L. Cui, L.S. Zhu, Anal. Chim. Acta 659 (2010) 144–150.
[31] A. Chunder, T. Pal, S.I. Khondaker, L. Zhai, J. Phys. Chem. C 114 (2010) 15129–15135.
[32] J.P. Mensing, T. Kerdcharoen, C. Sriprachuabwong, A. Wisitsoraat, D. Phokharatkul, T. Lomasa, A. Tuantranont, J. Mater. Chem. 22 (2012) 17094–17099.
[33] Y.Z. Zhang, G.Q. Mo, X.W. Li, J.S. Ye, J. Power Sources 197 (2012) 93–96.
[34] C.Z. Zhang, R. Hao, H. Yin, F. Liu, Y.L. Hou, Nanoscale 4 (2012) 7326–7329.
[35] Z.Y. Wang, N. Li, Z.J. Shi, Z.N. Gu, Nanotechnology 21 (2010) 175602/1–175602/4.
[36] Y. Wang, H.Z. Chen, H.Y. Li, M. Wang, Mater. Sci. Eng. B 117 (2005) 296–301.
[37] A. Baba, Y. Kanetsuna, S. Sriwichai, Y. Ohdaira, K. Shinbo, K. Kato, S. Phanichphant, F. Kaneko, Thin Solid Films 518 (2010) 2200–2205.
[38] A.C. Ferrari, J.C. Meyer, V. Scardaci, C. Casiraghi, M. Lazzeri, F. Mauri, S. Piscanec, D. Jiang, K.S. Novoselov, S. Roth, A.K. Geim, Phys. Rev. Lett. 97 (2006) 187401/1–187401/4.
[39] G.H. Zeng, Y.B. Xing, J. Gao, Z.Q. Wang, X. Zhang, Langmuir 26 (2010) 15022–15026.
[40] L.M. Malard, M.A. Pimenta, G. Dresselhaus, M.S. Dresselhaus, Phys. Rep. 473 (2009) 51–87.
[41] G.B. Zhu, X. Zhang, P.B. Gai, X.H. Zhang, J.H. Chen, Nanoscale 4 (2012) 5703–5709.
[42] M. Jahan, Q.L. Bao, K.P. Loh, J. Am. Chem. Soc. 134 (2012) 6707–6713.
[43] T.Y. Ma, Y.S. Wei, T.Z. Ren, L. Liu, Q. Guo, Z.Y. Yuan, ACS Appl. Mater. Interfaces 2 (2010) 3563–3571.
[44] M.Y. Zhang, C.L. Shao, Z.C. Guo, Z.Y. Zhang, J.B. Mu, T.P. Cao, Y.C. Liu, ACS Appl. Mater. Interfaces 3 (2011) 369–377.
[45] M.E. Ragoussi, J. Malig, G. Katsukis, B. Butz, E. Spiecker, G. de la Torre, T. Torres, D.M. Guldi, Angew. Chem. Int. Ed. 51 (2012) 6421–6425.
[46] H.L. Guo, X.F. Wang, Q.Y. Qian, F.B. Wang, X.H. Xia, ACS Nano 3 (2009) 2653–2659.
[47] G. Wang, J. Yang, J. Park, X. Gou, B. Wang, H. Liu, J. Yao, J. Phys. Chem. C 112 (2008) 8192–8195.
[48] L. Su, W.Z. Jia, L.C. Zhang, C. Beacham, H. Zhang, Y. Lei, J. Phys. Chem. C 114 (2010) 18121–18125.
[49] K.L. Nagashree, N.H. Raviraj, M.F. Ahmed, Electrochim. Acta 55 (2010) 2629–2635.
[50] Y.J. Kuang, Y. Cui, Y.S. Zhang, Y.M. Yu, X.H. Zhang, J.H. Chen, Chem. Eur. J. 18 (2012) 1522–1527.
[51] R.J. Liu, S.W. Li, X.L. Yu, G.J. Zhang, S.J. Zhang, J.N. Yao, L.J. Zhi, J. Mater. Chem. 22 (2012) 3319–3322.
[52] S.M. Choi, M.H. Seo, H.J. Kim, W.B. Kim, Carbon 49 (2011) 904–909.
[53] Y. Lu, R.G. Reddy, Int. J. Hydrogen Energy 33 (2008) 3930–3937.
[54] Y.W. Lee, A.R. Ko, S.B. Han, H.S. Kim, K.W. Park, Phys. Chem. Chem. Phys. 13 (2011) 5569–5572.
[55] R. Chetty, S. Kundu, W. Xia, M. Bron, W. Schuhmann, V. Chirila, W. Brandl, T. Reinecke, M. Muhler, Electrochim. Acta 54 (2009) 4208–4215.
[56] S. Sharma, A. Ganguly, P. Papakonstantinou, X.P. Miao, M.X. Li, J.L. Hutchison, M. Delichatsios, S. Ukleja, J. Phys. Chem. C 114 (2010) 19459–19466.

[57] G. García, J.F. Montano, A.H. Creus, E. Pastor, G.A. Planes, J. Power Sources 196 (2011) 2979–2986.
[58] C.Y. Du, T.S. Zhao, Z.X. Liang, J. Power Sources 176 (2008) 9–15.
[59] M. Carmo, M. Brandalise, A.O. Neto, E.V. Spinacé, A.D. Taylor, M. Linardi, J.G.R. Poço, Int. J. Hydrogen Energy 36 (2011) 14659–14667.
[60] G. de la Torre, C.G. Claessens, T. Torres, Chem. Commun. (2007) 2000–2015.
[61] C.G. Claessens, U. Hahn, T. Torres, Chem. Rec. 8 (2008) 75–97.
[62] X.C. Zhou, C.P. Liu, J.H. Liao, T.H. Lu, W. Xing, J. Power Sources 179 (2008) 481–488.
[63] L.Q. Hoa, M.C. Vestergaard, H. Yoshikawa, M. Satio, E. Tamiya, Electrochem. Commun. 13 (2011) 746–748.